

# Giant Enhancement of Unconventional Photon Blockade in a Dimer Chain

You Wang,<sup>1,\*</sup> W. Verstraelen,<sup>1,\*</sup> Baile Zhang,<sup>1,2,†</sup> Timothy C. H. Liew,<sup>1,3,‡</sup> and Y. D. Chong<sup>1,2,§</sup>

<sup>1</sup>*Division of Physics and Applied Physics, School of Physical and Mathematical Sciences,  
Nanyang Technological University, Singapore 637371, Singapore*

<sup>2</sup>*Centre for Disruptive Photonic Technologies, School of Physical and Mathematical Sciences,  
Nanyang Technological University, Singapore 637371, Singapore*

<sup>3</sup>*MajuLab, International Joint Research Unit UMI 3654,  
CNRS, Université Côte d'Azur, Sorbonne Université,  
National University of Singapore, Nanyang Technological University, Singapore*  
(Dated: October 11, 2021)

Unconventional photon blockade refers to the suppression of multi-photon states in weakly nonlinear optical resonators via the destructive interference of different excitation pathways. It has been studied in a pair of coupled nonlinear resonators and other few-mode systems. Here, we show that unconventional photon blockade can be greatly enhanced in a chain of coupled resonators. Specifically, the strength of the nonlinearity in each resonator needed to achieve unconventional photon blockade is suppressed exponentially with lattice size. The analytic derivation, based on a weak drive approximation, is validated by wavefunction Monte Carlo simulations. These findings show that customized lattices of coupled resonators can be powerful tools for controlling multi-photon quantum states.

Photon blockade—the use of optical nonlinearity to suppress multi-photon quantum states—is a mechanism for generating nonclassical light through classical optical illumination [1–4], with applications in quantum computing, quantum simulation, and other emerging quantum technologies [5–12]. The conventional photon blockade effect requires strong optical nonlinearities, as it relies on interactions between resonant single-photon states and off-resonant multi-photon states, so the interaction strength has to be much larger than the cavity decay rate. This regime can be achieved in cavity QED systems [6, 13–23], superconducting circuits [24, 25], optomechanical resonators [25–28], and other systems [29, 30]. Weak nonlinearities, however, are much easier to realize, such as in resonators made of common nonlinear optical materials. Remarkably, it is possible to efficiently suppress multi-photon states even in the weakly nonlinear regime, through the phenomenon of unconventional photon blockade (UPB). Liew and Savona showed some years ago that in a system of two coupled nonlinear resonators, careful parameter tuning can enable destructive interference between different excitation pathways for the formation of two-photon states in the signal resonator, even when the photon interaction strength is smaller than the cavity decay rate [31]. Subsequently, the conditions for UPB to occur have been extensively studied [32–37], and the phenomenon has been realized in experiments [38, 39]. Other ways of realizing UPB using different setups and different quantum interference schemes have also been proposed [33, 40–53], and similar ideas have been explored for other forms of multi-photon state control in weakly nonlinear systems, such as for creating entangled photon sources [54, 55].

In the context of classical optics and photonics, synthetic lattices such as photonic crystals [56–58] and pho-

tonic metamaterials [59–62] have proven to be versatile platforms for wave manipulation. By offering a richer set of customizable degrees of freedom, such as lattice symmetries, they have the potential to outperform devices composed of individual or a few coupled optical cavities, or even access qualitatively different behaviors. For instance, photonic lattices can exhibit bound states in the continuum, whose decay rates vanish due to destructive interference of numerous decay pathways [63].

In this Letter, we show that a lattice of coupled resonators can achieve UPB at much lower levels of optical nonlinearity than in previously-studied two-resonator setups. We consider resonators arranged in a dimer chain, or Su-Schrieffer-Heeger (SSH) lattice [64], a one-dimensional model lattice whose single-particle properties have been extensively studied. By extending the analysis to two-photon states and exploiting the lattice's various features, including its chiral symmetry, we derive analytic expressions for the one- and two-photon quantum amplitudes to leading order in the inter-cell coupling. Remarkably, we find that the nonlinear Kerr coefficient necessary for UPB in a given signal resonator is suppressed exponentially in the total number of sites. The theory predicts the necessary resonator frequency detunings and cavity decay rates, which form a striking pattern of complex roots in a 2D parameter space. For the limiting case of just two resonators, our formulas reproduce previously-reported results [33]. We have also performed wavefunction Monte Carlo (WFMC) simulations of the multi-photon system, which give good agreement with the analytic results, and help quantify the limits on photon antibunching imposed by pure dephasing. Recently, two-mode UPB has been demonstrated with quantum dot cavities [38] and superconducting circuits [39], and our findings may help in designing lattice-based single-

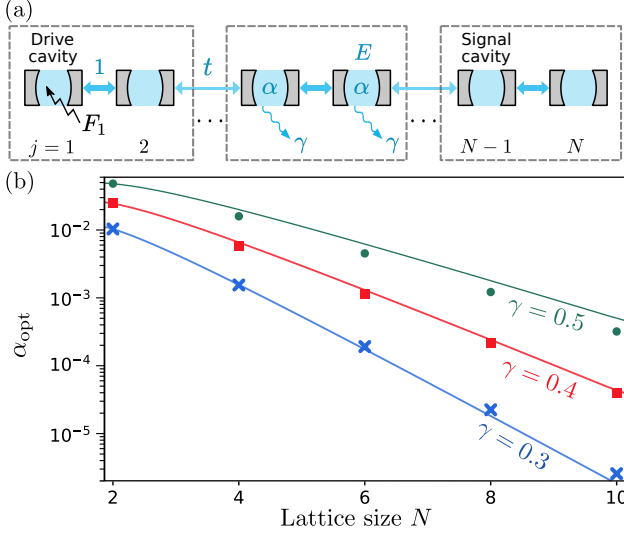


FIG. 1. (a) Schematic of a dimer chain lattice of optical cavities. The cavity on site  $j = 1$  is coherently driven, and site  $N - 1$  is the signal resonator. Each cavity has single-photon energy  $E$ , Kerr coefficient  $\alpha$ , and decay rate  $\gamma$ . Dashed boxes indicate the unit cells; the intra- and inter-cell couplings are 1 and  $t$  respectively. (b) Optimum Kerr coefficient for different lattice lengths with  $t = 0.1$  and  $\gamma = 0.3, 0.4, 0.5$ . The solid curves correspond to the analytic approximation (17), while the discrete data points are calculated numerically from the weak drive equations.

photon sources on weakly-nonlinear platforms such as silicon photonics [41, 65].

Consider coupled optical resonators with identical physical properties and weak Kerr-type nonlinearity, arranged in a dimer chain (or SSH lattice [64]) as shown in Fig. 1(a). The number of sites,  $N$ , is even. In the absence of driving and dissipation, the Hamiltonian is  $\mathcal{H}_0 = \mathcal{H}_c + \mathcal{H}_p + \mathcal{H}_{nl}$ , where

$$\mathcal{H}_c = \left( \sum_{j=1}^{N/2} a_{2j-1}^\dagger a_{2j} + t \sum_{j=1}^{N/2-1} a_{2j}^\dagger a_{2j+1} \right) + \text{h.c.} \quad (1)$$

$$\mathcal{H}_p = E \sum_{j=1}^N a_j^\dagger a_j, \quad \mathcal{H}_{nl} = \alpha \sum_{j=1}^N a_j^\dagger a_j^\dagger a_j a_j.$$

Here,  $a_j^{(\dagger)}$  is the photon annihilation (creation) operator on site  $j$ ,  $t$  is the intercell hopping (with the intra-cell hopping normalized to unity),  $E$  is the on-site single-photon energy,  $\alpha \in \mathbb{R}$  is the Kerr coefficient, and “h.c.” stands for the Hermitian conjugate. Here we choose positive couplings; negative couplings can be equivalently handled by redefining the operators on even sites. Note that although the SSH model is well-known for the existence of “topologically protected” single-particle eigenstates at boundaries and domain walls, this behavior is not used in the present work; we exploit its other features, such as the chiral symme-

try of the lattice. We consider a chain with no domain walls, and (since  $N$  is even) no single-particle topological eigenstates.

Let the sites be coherently driven by the Hamiltonian

$$\mathcal{H}_d = \sum_{j=1}^N F_j a_j^\dagger + \text{h.c.}, \quad (2)$$

where  $F_j$  is the excitation coefficient on site  $j$ . Fig. 1(a) depicts the case where only the first site is driven,  $F_j = F_1 \delta_{1j}$ . The evolution of the density matrix  $\rho$  is given by the Lindblad master equation [66]

$$i\hbar \frac{d\rho}{dt} = [\mathcal{H}_{\text{tot}}, \rho] + \frac{i\gamma}{2} \sum_{j=1}^N \left( 2a_j \rho a_j^\dagger - a_j^\dagger a_j \rho - \rho a_j^\dagger a_j \right), \quad (3)$$

where  $\mathcal{H}_{\text{tot}} = \mathcal{H}_0 + \mathcal{H}_d$ . The terms in parentheses represent the interaction of the system with the environment in the form of on-site losses, giving rise to (i) a deterministic decay and (ii) stochastic quantum jumps stemming from the fluctuation-dissipation theorem. Both of these effects will be accounted for when we later solve Eq. (3) using stochastic WFMC simulations [67–70]. For now, however, we pursue an approximate analytic solution by neglecting the fluctuations, and absorbing the deterministic decay terms into the Hamiltonian. Let us define

$$z = E - \frac{i\gamma}{2}, \quad \mathcal{H}'_p = z \sum_{j=1}^N a_j^\dagger a_j, \quad (4)$$

and consider the semiclassical regime where the time evolution is well described by the Schrödinger equation with the non-Hermitian Hamiltonian  $\mathcal{H} = \mathcal{H}_c + \mathcal{H}'_p + \mathcal{H}_{nl}$ . Flayac and Savona have argued that this is valid in the “weak drive” limit  $F_j \rightarrow 0$ , since stochastic jumps are rare when photon occupation numbers are low [43].

The steady state solution has the form

$$|\psi\rangle = \sum_{k=0}^{\infty} |\psi^{(k)}\rangle, \quad (5)$$

where  $|\psi^{(k)}\rangle$  is the projection of the full wavefunction into the  $k$ -photon subspace. In the weak drive limit, the amplitude for the higher photon number states is negligible. Truncating at  $k = 2$ , we obtain [71]

$$|\psi^{(1)}\rangle = -\mathcal{H}^{-1} \mathcal{H}_+ |\psi^{(0)}\rangle, \quad (6)$$

$$|\psi^{(2)}\rangle = -\mathcal{H}^{-1} \mathcal{H}_+ |\psi^{(1)}\rangle, \quad (7)$$

where  $\mathcal{H}_+ = \sum_j F_j a_j^\dagger$ . For  $k = 1$ , we adopt the eigenstate basis of  $\mathcal{H}_c^{(1)}$  (the projection of  $\mathcal{H}_c$  to the 1-photon subspace), defined by

$$\mathcal{H}_c^{(1)} |\varphi_n\rangle = \epsilon_n |\varphi_n\rangle. \quad (8)$$

Hence, the solution to Eq. (6) can be written as

$$|\psi^{(1)}\rangle = \sum_n \frac{f_n |\varphi_n\rangle}{z + \epsilon_n}, \quad f_n = \sum_{j=1}^N F_j \langle \varphi_n | j \rangle, \quad (9)$$

where  $|j\rangle \equiv a_j^\dagger |\psi^{(0)}\rangle$ . Details of the derivation are given in the Supplemental Materials [71]. Next, for  $k = 2$ , we define a basis formed by tensor products of the single-particle eigenstates,  $|\varphi_{mn}\rangle \equiv |\varphi_m\rangle \otimes |\varphi_n\rangle$ , and seek perturbative solutions to Eq. (7) of the form

$$|\psi^{(2)}\rangle \approx |\psi_0^{(2)}\rangle + \alpha |\psi_1^{(2)}\rangle, \quad (10)$$

where the solution in the absence of interactions is

$$|\psi_0^{(2)}\rangle = \frac{1}{\sqrt{2}} \sum_{mn} \frac{f_m f_n}{(z + \epsilon_m)(z + \epsilon_n)} |\varphi_{mn}\rangle, \quad (11)$$

and the perturbative correction can be shown to be [71]

$$|\psi_1^{(2)}\rangle = \sum_{imnpq} |\varphi_{mn}\rangle \frac{-\sqrt{2} f_p f_q \langle \varphi_{mn} | i, i \rangle \langle i, i | \varphi_{pq} \rangle}{(z + \epsilon_p)(z + \epsilon_q)(2z + \epsilon_m + \epsilon_n)}, \quad (12)$$

where  $|i, i\rangle \equiv |i\rangle \otimes |i\rangle$ .

We now let only the first site be driven, so that  $f_n = F_1 \langle \varphi_n | 1 \rangle$ . The  $N = 2$  lattice, corresponding to a single dimer, has previously been shown [31] to exhibit UPB in site 1, which serves as both the drive and signal resonator. For larger  $N$ , we will demonstrate enhanced UPB on a designated signal resonator on site  $N - 1$  of the chain (i.e., one site away from the end of the chain, opposite to the drive cavity), as shown in Fig. 1(a). UPB shall be achieved if the equal time second order photon correlation in the signal resonator,

$$g_s^{(2)}(0) = 2 \frac{|\langle N - 1, N - 1 | \psi^{(2)} \rangle|^2}{|\langle N - 1 | \psi^{(1)} \rangle|^4}, \quad (13)$$

vanishes. Note that plugging only Eq. (11) into Eq. (13) gives  $g_s^{(2)}(0) = 1$  (i.e., in the linear regime the emission is always coherent).

If the intercell coupling is weak ( $t \ll 1$ ), we can estimate the two-photon state by applying Laurent series expansions to Eqs. (11) and (12) in the domain  $t < |z| < 1$ . The derivation, given in the Supplemental Materials [71], utilizes the chiral symmetry of  $\mathcal{H}_c^{(1)}$ , which ensures that the single-photon spectrum is symmetric around  $E = 0$ . The result is

$$\langle N - 1, N - 1 | \psi_0^{(2)} \rangle \approx \frac{F_1^2}{\sqrt{2}} t^{N-2} z^2, \quad (14)$$

$$\langle N - 1, N - 1 | \psi_1^{(2)} \rangle \approx \frac{F_1^2}{\sqrt{2}} \frac{(-1)^{\frac{N}{2}+1} (N - 3)!! t^{N-2}}{(N - 2)!! (2z)^{N-1}}.$$

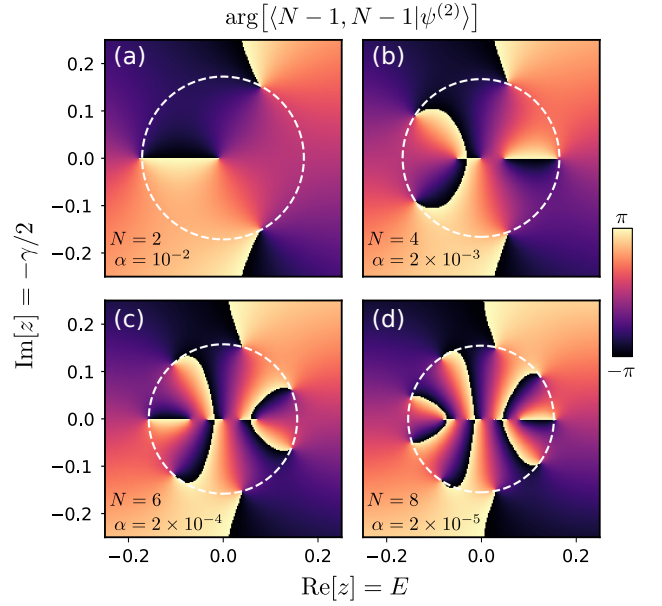


FIG. 2. Complex argument of  $\langle N - 1, N - 1 | \psi^{(2)} \rangle$ , the two-photon amplitude in the signal resonator, plotted versus  $\text{Re}[z] = E$  and  $\text{Im}[z] = -\gamma/2$ . The heat maps are obtained by solving the weak drive equations numerically, without the analytic approximations, using intracell coupling  $t = 0.1$  and different values of  $N, \alpha$ : (a)  $N = 2$  with  $\alpha = 10^{-2}$ , (b)  $N = 4$  with  $\alpha = 2 \times 10^{-3}$ , (c)  $N = 6$  with  $\alpha = 2 \times 10^{-4}$ , and (d)  $N = 8$  with  $\alpha = 2 \times 10^{-5}$ . The dashed circles indicate the optimal values of  $|z|$  predicted by the analytic expression (15).

Referring to Eq. (10), UPB is achieved when

$$\alpha \approx \frac{(-1)^{\frac{N}{2}}}{4} \frac{(N - 2)!!}{(N - 3)!!} (2z)^{N+1}. \quad (15)$$

Notably, this is independent of the drive amplitude  $F_1$ .

Since  $\alpha \in \mathbb{R}$ ,  $z/|z|$  must be one of the  $(N + 1)$  complex roots of  $(-1)^{N/2}$  or  $(-1)^{N/2+1}$  depending on the sign of  $\alpha$ . We require  $\text{Im}(z) = -\gamma/2 < 0$  (i.e., the resonators are subject to loss rather than gain), and select the root with the most negative imaginary part. This corresponds to the experimentally preferred situation where  $\alpha/\gamma$ , the nonlinearity strength relative to the cavity decay rate, is minimal. (Choosing a different root yields only small modifications to the following results.) Here and in the following, we restrict our discussion to  $\alpha > 0$ . Note that our theory also applies for  $\alpha < 0$ . The results for  $E$  and  $\alpha$ , expressed in terms of  $\gamma$ , are

$$E = \frac{\gamma}{2} \cot \theta, \quad (16)$$

$$\alpha = \frac{1}{4} \frac{(N - 2)!!}{(N - 3)!!} (\gamma \csc \theta)^{N+1}, \quad (17)$$

$$\theta = \frac{N}{N + 1} \frac{\pi}{2}. \quad (18)$$

For  $N = 2$ , this reproduces the previously-derived single-dimer result [33]. For larger  $N$ , given any decay rate  $\gamma$

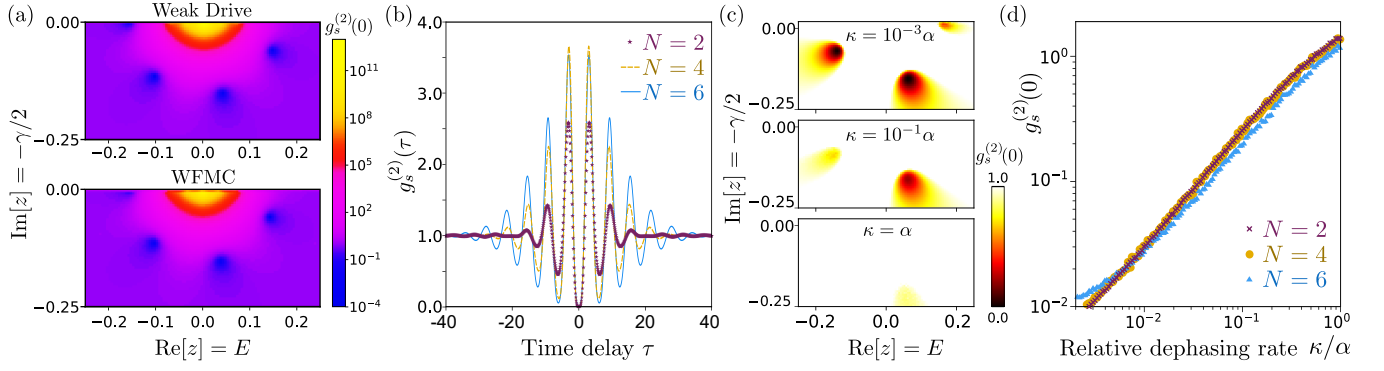


FIG. 3. Wavefunction Monte Carlo (WFMC) results. In all subplots, we take  $t = 0.1$  and for lattices of size  $N = 2, 4, 6$ , we set  $\alpha = 10^{-2}, 2 \times 10^{-3}, 2 \times 10^{-4}$  respectively. (a) Equal time second order correlation  $g_s^{(2)}(0)$  versus  $z = E - i\gamma/2$  for a lattice of size  $N = 6$ , obtained using the weak drive equations without series expansions (upper panel), and using WFMC simulations with drive amplitude  $F_1 = 10^{-4}$  (lower panel). (b) WFMC results for the unequal time correlation  $g_s^{(2)}(\tau)$ . For each  $N$ , the value of  $z$  is chosen to minimize  $g_s^{(2)}(0)$ , and is located by doing simulations with different  $z$  on a discrete grid. The horizontal axis has units of  $\hbar$  over the intracell coupling. In (a) and (b), the WFMC simulations do not include pure dephasing. (c) Plots of  $g_s^{(2)}(0)$  versus  $z$  for a lattice with  $N = 4$ , obtained using WFMC simulations with dephasing rates  $\kappa = 0.001\alpha, 0.1\alpha, \alpha$  (top to bottom). To distinguish the local minima more clearly, all regions for which  $g_s^{(2)}(0) \geq 1$  are colored white. (d) Dependence of  $g_s^{(2)}(0)$  on  $\kappa/\alpha$  for lattices of size  $N = 2, 4, 6$ , using the same values of  $z$  as in (b).

smaller than the intercell coupling strength (i.e.,  $\gamma < 1$ ), Eq. (17) states that the nonlinearity strength  $\alpha$  required for UPB decreases exponentially with the lattice size  $N$ . This is the primary finding of the present work.

Instead of using the series expansions, we can also solve the single-photon eigenproblem (8) numerically, and plug the results into the weak drive equations (9) and (11)–(12) to obtain the single-photon and two-photon wavefunctions. This is more efficient than directly solving Eqs. (6)–(7) since it avoids performing a matrix inversion for each  $z$ . Fig. 1(b) plots the optimal Kerr coefficients versus lattice size  $N$ , as given by the analytic expression derived from the series expansions (solid curves) and the numerical solutions to the weak drive equations (discrete points). The analytic expression agrees well with the numerical results.

It is worth noting that the vanishing of the two-photon signal  $\langle N-1, N-1 | \psi^{(2)} \rangle$  is due to the presence of exact zeros in the complex  $z$  plane. It is a feature of the weak drive equations themselves, and is not an artifact of the series expansions leading up to the analytic result (17), which merely identify approximate (but accurate) locations for the zeros. To show this, Fig. 2 plots the complex argument of  $\langle N-1, N-1 | \psi^{(2)} \rangle$  versus  $z$ , obtained numerically from the weak drive equations for different  $N$ . Here and in the following numerical examples, we take  $t = 0.1$  and choose different values of  $\alpha$  for each  $N$ . We observe phase singularities at discrete  $z$  points, corresponding to analytic zeros. These occur in the predicted pattern of roots of  $(-1)^{N/2}$ , and with increasing  $N$  we see that smaller values of  $\alpha$  are required for the zeros to appear at comparable  $|z|$ , as expected.

To verify the results obtained from the weak drive ap-

proximation, we performed WFMC simulations [67–70], which solve the Lindblad equation (3) including the effects of stochastic quantum jumps. Fig. 3(a) compares the equal time second order correlations calculated by the two methods, for a lattice of  $N = 6$  sites. The WFMC simulations were performed using per-site Fock cutoffs chosen to balance accuracy and computational cost [71]; the results shown here were obtained with drive amplitude  $F_1 = 10^{-4}$ , but almost identical outcomes can be obtained for other values of  $F_1 \ll 1$  [71]. The WFMC and weak drive calculations produce very similar results, particularly with regard to the parameter values where photon antibunching occurs. The results for lattices of size  $N = 2$  and  $N = 4$  show similar good agreement, as shown in the Supplemental Materials [71].

Fig. 3(b) shows the unequal time second order correlation  $g_s^{(2)}(\tau)$  [71], calculated with WFMC for lattices of size  $N = 2, 4, 6$  (each lattice is individually tuned to its optimal point). For  $N = 2$  (the case of a single dimer), the correlation has previously been shown to oscillate with  $\tau$  [31]. The behavior for larger values of  $N$  is similar, with the oscillation frequency not significantly influenced by  $N$ .

In systems subject to significant environmental perturbations, UPB may be constrained by pure dephasing, distinct from the dissipation-induced quantum jumps considered thus far. To investigate this, we performed a set of WFMC simulations with the term

$$i\frac{\kappa}{2} \sum_j (2a_j^\dagger a_j \rho a_j^\dagger a_j - a_j^\dagger a_j a_j^\dagger a_j \rho - \rho a_j^\dagger a_j a_j^\dagger a_j) \quad (19)$$

added to the Lindblad master equation [31]. Fig. 3(c) shows the  $z$ -dependence of  $g_s^{(2)}(0)$  for  $N = 4$  using the

dephasing rates  $\kappa = 10^{-3}\alpha$ ,  $0.1\alpha$ , and  $\alpha$ . We see that pure dephasing, if excessively strong, “smears out” the zeros of  $g_s^{(2)}(0)$ . In Fig. 3(d), we plot the dependence of  $g_s^{(2)}(0)$  on the dephasing rate for lattices of size  $N = 2, 4$ , and  $6$ . These results indicate that photon antibunching requires  $\kappa$  to be small compared to  $\alpha$ . This will have to be taken into account to achieve UPB in large- $N$  lattices with extremely weak nonlinearities.

Our finding of exponential enhancement of UPB in a dimer chain, one of the simplest lattice models, points to exciting opportunities for using photonic lattices to manipulate multi-photon quantum states. In the future, related effects could be explored in more complicated systems such as two-dimensional lattices, as well as exploiting special lattice phenomena such as topologically protected single-photon states [72–75]. It would also be interesting to use these ideas to implement single-photon sources using silicon photonics, or other photonic platforms with weak optical nonlinearities.

This work was supported by Singapore MOE Academic Research Fund Tier 3 Grant MOE2016-T3-1-006, Tier 1 Grants RG187/18(S) and RG148/20, and Tier 2 Grants MOE2019-T2-2-085, MOE2019-T2-1-004

---

\* These authors contributed equally.

† blzhang@ntu.edu.sg

‡ timothyliw@ntu.edu.sg

§ yidong@ntu.edu.sg

- [1] L. Tian and H. J. Carmichael, Quantum trajectory simulations of two-state behavior in an optical cavity containing one atom, *Phys. Rev. A* **46**, R6801 (1992).
- [2] W. Leoński and R. Tanaś, Possibility of producing the one-photon state in a kicked cavity with a nonlinear Kerr medium, *Phys. Rev. A* **49**, R20 (1994).
- [3] A. Imamoglu, H. Schmidt, G. Woods, and M. Deutsch, Strongly interacting photons in a nonlinear cavity, *Phys. Rev. Lett.* **79**, 1467 (1997).
- [4] P. Lodahl, S. Mahmoodian, and S. Stobbe, Interfacing single photons and single quantum dots with photonic nanostructures, *Rev. Mod. Phys.* **87**, 347 (2015).
- [5] E. Knill, R. Laflamme, and G. J. Milburn, A scheme for efficient quantum computation with linear optics, *Nature* **409**, 46 (2001).
- [6] K. M. Birnbaum, A. Boca, R. Miller, A. D. Boozer, T. E. Northup, and H. J. Kimble, Photon blockade in an optical cavity with one trapped atom, *Nature* **436**, 87 (2005).
- [7] M. J. Hartmann, F. G. S. L. Brandão, and M. B. Plenio, Strongly interacting polaritons in coupled arrays of cavities, *Nat. Phys.* **2**, 849 (2006).
- [8] A. D. Greentree, C. Tahan, J. H. Cole, and L. C. L. Hollenberg, Quantum phase transitions of light, *Nat. Phys.* **2**, 856 (2006).
- [9] P. Kok, W. J. Munro, K. Nemoto, T. C. Ralph, J. P. Dowling, and G. J. Milburn, Linear optical quantum computing with photonic qubits, *Rev. Mod. Phys.* **79**, 135 (2007).
- [10] D. G. Angelakis, M. F. Santos, and S. Bose, Photon-blockade-induced mott transitions and  $xy$  spin models in coupled cavity arrays, *Phys. Rev. A* **76**, 031805 (2007).
- [11] R. O. Umucahlar and I. Carusotto, Fractional quantum hall states of photons in an array of dissipative coupled cavities, *Phys. Rev. Lett.* **108**, 206809 (2012).
- [12] C. Noh and D. G. Angelakis, Quantum simulations and many-body physics with light, *Rep. Progr. Phys.* **80**, 016401 (2016).
- [13] B. Dayan, A. S. Parkins, T. Aoki, E. P. Ostby, K. J. Vahala, and H. J. Kimble, A photon turnstile dynamically regulated by one atom, *Science* **319**, 1062 (2008).
- [14] C. Hamsen, K. N. Tolazzi, T. Wilk, and G. Rempe, Two-photon blockade in an atom-driven cavity qed system, *Phys. Rev. Lett.* **118**, 133604 (2017).
- [15] P. Michler, A. Kiraz, C. Becher, W. V. Schoenfeld, P. M. Petroff, L. Zhang, E. Hu, and A. Imamoglu, A quantum dot single-photon turnstile device, *Science* **290**, 2282 (2000).
- [16] A. Faraon, I. Fushman, D. Englund, N. Stoltz, P. Petroff, and J. Vučković, Coherent generation of non-classical light on a chip via photon-induced tunnelling and blockade, *Nat. Phys.* **4**, 859 (2008).
- [17] J. Claudon, J. Bleuse, N. S. Malik, M. Bazin, P. Jaffrennou, N. Gregersen, C. Sauvan, P. Lalanne, and J.-M. Gérard, A highly efficient single-photon source based on a quantum dot in a photonic nanowire, *Nat. Photon.* **4**, 174 (2010).
- [18] Y.-M. He, Y. He, Y.-J. Wei, D. Wu, M. Atatüre, C. Schneider, S. Höfling, M. Kamp, C.-Y. Lu, and J.-W. Pan, On-demand semiconductor single-photon source with near-unity indistinguishability, *Nat. Nanotech.* **8**, 213 (2013).
- [19] K. H. Madsen, S. Ates, J. Liu, A. Javadi, S. M. Albrecht, I. Yeo, S. Stobbe, and P. Lodahl, Efficient out-coupling of high-purity single photons from a coherent quantum dot in a photonic-crystal cavity, *Phys. Rev. B* **90**, 155303 (2014).
- [20] M. Gschrey, A. Thoma, P. Schnauber, M. Seifried, R. Schmidt, B. Wohlfeil, L. Krüger, J. H. Schulze, T. Heindel, S. Burger, F. Schmidt, A. Strittmatter, S. Rodt, and S. Reitzenstein, Highly indistinguishable photons from deterministic quantum-dot microlenses utilizing three-dimensional in situ electron-beam lithography, *Nat. Comm.* **6**, 7662 (2015).
- [21] N. Somaschi, V. Giesz, L. D. Santis, J. C. Lored, M. P. Almeida, G. Hornecker, S. L. Portalupi, T. Grange, C. Antón, J. Demory, C. Gómez, I. Sagnes, N. D. Lanzillotti-Kimura, A. Lemaître, A. Auffeves, A. G. White, L. Lanco, and P. Senellart, Near-optimal single-photon sources in the solid state, *Nature Photonics* **10**, 340 (2016).
- [22] C. Dory, K. A. Fischer, K. Müller, K. G. Lagoudakis, T. Sarmiento, A. Rundquist, J. L. Zhang, Y. Kelaita, N. V. Saprà, and J. Vučković, Tuning the photon statistics of a strongly coupled nanophotonic system, *Phys. Rev. A* **95**, 023804 (2017).
- [23] N. Jia, N. Schine, A. Georgakopoulos, A. Ryou, L. W. Clark, A. Sommer, and J. Simon, A strongly interacting polaritonic quantum dot, *Nat. Phys.* **14**, 550 (2018).
- [24] C. Lang, D. Bozyigit, C. Eichler, L. Steffen, J. M. Fink, A. A. Abdumalikov, M. Baur, S. Filipp, M. P. da Silva, A. Blais, and A. Wallraff, Observation of resonant photon blockade at microwave frequencies using correlation function measurements, *Phys. Rev. Lett.* **106**, 243601 (2011).

- [25] X. Wang, A. Miranowicz, H.-R. Li, and F. Nori, Multiple-output microwave single-photon source using superconducting circuits with longitudinal and transverse couplings, *Phys. Rev. A* **94**, 053858 (2016).
- [26] P. Rabl, Photon blockade effect in optomechanical systems, *Phys. Rev. Lett.* **107**, 063601 (2011).
- [27] X.-W. Xu, A.-X. Chen, and Y.-x. Liu, Phonon blockade in a nanomechanical resonator resonantly coupled to a qubit, *Phys. Rev. A* **94**, 063853 (2016).
- [28] M.-A. Lemonde, N. Didier, and A. A. Clerk, Enhanced nonlinear interactions in quantum optomechanics via mechanical amplification, *Nat. Comm.* **7**, 11338 (2016).
- [29] A. Majumdar, M. Bajcsy, A. Rundquist, and J. Vučković, Loss-enabled sub-poissonian light generation in a bimodal nanocavity, *Phys. Rev. Lett.* **108**, 183601 (2012).
- [30] A. Majumdar and D. Gerace, Single-photon blockade in doubly resonant nanocavities with second-order nonlinearity, *Phys. Rev. B* **87**, 235319 (2013).
- [31] T. C. H. Liew and V. Savona, Single photons from coupled quantum modes, *Phys. Rev. Lett.* **104**, 183601 (2010).
- [32] S. Ferretti, L. C. Andreani, H. E. Türeci, and D. Gerace, Photon correlations in a two-site nonlinear cavity system under coherent drive and dissipation, *Phys. Rev. A* **82**, 013841 (2010).
- [33] M. Bamba, A. Imamoğlu, I. Carusotto, and C. Ciuti, Origin of strong photon antibunching in weakly nonlinear photonic molecules, *Phys. Rev. A* **83**, 021802 (2011).
- [34] M. Bamba and C. Ciuti, Counter-polarized single-photon generation from the auxiliary cavity of a weakly nonlinear photonic molecule, *Appl. Phys. Lett.* **99**, 171111 (2011).
- [35] H. Flayac and V. Savona, Input-output theory of the unconventional photon blockade, *Phys. Rev. A* **88**, 033836 (2013).
- [36] X.-W. Xu and Y. Li, Strong photon antibunching of symmetric and antisymmetric modes in weakly nonlinear photonic molecules, *Phys. Rev. A* **90**, 033809 (2014).
- [37] M.-A. Lemonde, N. Didier, and A. A. Clerk, Antibunching and unconventional photon blockade with gaussian squeezed states, *Phys. Rev. A* **90**, 063824 (2014).
- [38] H. J. Snijders, J. A. Frey, J. Norman, H. Flayac, V. Savona, A. C. Gossard, J. E. Bowers, M. P. van Exter, D. Bouwmeester, and W. Löffler, Observation of the unconventional photon blockade, *Phys. Rev. Lett.* **121**, 043601 (2018).
- [39] C. Vaneph, A. Morvan, G. Aiello, M. Féchant, M. Aprili, J. Gabelli, and J. Estève, Observation of the unconventional photon blockade in the microwave domain, *Phys. Rev. Lett.* **121**, 043602 (2018).
- [40] D. Gerace and V. Savona, Unconventional photon blockade in doubly resonant microcavities with second-order nonlinearity, *Phys. Rev. A* **89**, 031803 (2014).
- [41] H. Flayac, D. Gerace, and V. Savona, An all-silicon single-photon source by unconventional photon blockade, *Scientific Reports* **5**, 11223 (2015).
- [42] H. Z. Shen, Y. H. Zhou, and X. X. Yi, Tunable photon blockade in coupled semiconductor cavities, *Phys. Rev. A* **91**, 063808 (2015).
- [43] H. Flayac and V. Savona, Unconventional photon blockade, *Phys. Rev. A* **96**, 053810 (2017).
- [44] G. Wang, H. Z. Shen, C. Sun, C. Wu, J.-L. Chen, and K. Xue, Unconventional photon blockade in weakly nonlinear photonic molecules with bilateral drive, *Journal of Modern Optics* **64**, 583 (2017).
- [45] B. Sarma and A. K. Sarma, Quantum-interference-assisted photon blockade in a cavity via parametric interactions, *Phys. Rev. A* **96**, 053827 (2017).
- [46] S. Ghosh and T. C. H. Liew, Single photons from a gain medium below threshold, *Phys. Rev. B* **97**, 241301 (2018).
- [47] H. Z. Shen, S. Xu, Y. H. Zhou, G. Wang, and X. X. Yi, Unconventional photon blockade from bimodal driving and dissipations in coupled semiconductor microcavities, *Journal of Physics B: Atomic, Molecular and Optical Physics* **51**, 035503 (2018).
- [48] B. Sarma and A. K. Sarma, Unconventional photon blockade in three-mode optomechanics, *Phys. Rev. A* **98**, 013826 (2018).
- [49] S. Ghosh and T. C. H. Liew, Dynamical blockade in a single-mode bosonic system, *Phys. Rev. Lett.* **123**, 013602 (2019).
- [50] H. Carmichael, R. Brecha, and P. Rice, Quantum interference and collapse of the wavefunction in cavity QED, *Optics Communications* **82**, 73 (1991).
- [51] M. Radulaski, K. A. Fischer, K. G. Lagoudakis, J. L. Zhang, and J. Vučković, Photon blockade in two-emitter-cavity systems, *Phys. Rev. A* **96**, 011801 (2017).
- [52] K. Kamide, Y. Ota, S. Iwamoto, and Y. Arakawa, Method for generating a photonic noon state with quantum dots in coupled nanocavities, *Phys. Rev. A* **96**, 013853 (2017).
- [53] E. Zubizarreta Casalengua, J. C. López Carreño, F. P. Laussy, and E. d. Valle, Conventional and unconventional photon statistics, *Laser & Photonics Reviews* **14**, 1900279 (2020).
- [54] T. C. H. Liew and V. Savona, Quantum entanglement in nanocavity arrays, *Phys. Rev. A* **85**, 050301 (2012).
- [55] T. C. H. Liew and V. Savona, Multimode entanglement in coupled cavity arrays, *New Journal of Physics* **15**, 025015 (2013).
- [56] S. John, Strong localization of photons in certain disordered dielectric superlattices, *Phys. Rev. Lett.* **58**, 2486 (1987).
- [57] E. Yablonovitch, Inhibited spontaneous emission in solid-state physics and electronics, *Phys. Rev. Lett.* **58**, 2059 (1987).
- [58] J. D. Joannopoulos, S. G. Johnson, J. N. Winn, and R. D. Meade, *Photonic Crystals* (Princeton University Press, 2008).
- [59] J. B. Pendry, Negative refraction makes a perfect lens, *Phys. Rev. Lett.* **85**, 3966 (2000).
- [60] E. Shamonina and L. Solymar, Metamaterials: How the subject started, *Metamaterials* **1**, 12 (2007).
- [61] J. Valentine, S. Zhang, T. Zentgraf, E. Ulin-Avila, D. A. Genov, G. Bartal, and X. Zhang, Three-dimensional optical metamaterial with a negative refractive index, *Nature* **455**, 376 (2008).
- [62] E. Cubukcu, K. Aydin, E. Ozbay, S. Foteinopoulou, and C. M. Soukoulis, Negative refraction by photonic crystals, *Nature* **423**, 604 (2003).
- [63] C. W. Hsu, B. Zhen, A. D. Stone, J. D. Joannopoulos, and M. Soljačić, Bound states in the continuum, *Nature Reviews Materials* **1**, 16048 (2016).
- [64] W. P. Su, J. R. Schrieffer, and A. J. Heeger, Solitons in polyacetylene, *Phys. Rev. Lett.* **42**, 1698 (1979).
- [65] S. Ferretti, V. Savona, and D. Gerace, Optimal antibunching in passive photonic devices based on coupled nonlinear resonators, *New Journal of Physics* **15**, 025012 (2013).

- (2013).
- [66] H. Breuer and F. Petruccione, *The Theory of Open Quantum Systems* (OUP Oxford, 2007); H. Carmichael, *Statistical Methods in Quantum Optics 2: Non-Classical Fields* (Springer Berlin Heidelberg, 2007).
  - [67] R. Dum, A. S. Parkins, P. Zoller, and C. W. Gardiner, Monte carlo simulation of master equations in quantum optics for vacuum, thermal, and squeezed reservoirs, *Phys. Rev. A* **46**, 4382 (1992).
  - [68] K. Mølmer, Y. Castin, and J. Dalibard, Monte carlo wave-function method in quantum optics, *J. Opt. Soc. Am. B* **10**, 524 (1993).
  - [69] H. Carmichael, *An open systems approach to quantum optics* (Springer, 1993).
  - [70] A. Barchielli and V. P. Belavkin, Measurements continuous in time and a posteriori states in quantum mechanics, *Journal of Physics A: Mathematical and General* **24**, 1495 (1991).
  - [71] See supplementary material.
  - [72] Z. Wang, Y. Chong, J. D. Joannopoulos, and M. Soljačić, Observation of unidirectional backscattering-immune topological electromagnetic states, *Nature* **461**, 772 (2009).
  - [73] T. Ozawa, H. M. Price, A. Amo, N. Goldman, M. Hafezi, L. Lu, M. C. Rechtsman, D. Schuster, J. Simon, O. Zilberberg, and I. Carusotto, Topological photonics, *Rev. Mod. Phys.* **91**, 015006 (2019).
  - [74] V. Peano, M. Houde, F. Marquardt, and A. A. Clerk, Topological quantum fluctuations and traveling wave amplifiers, *Phys. Rev. X* **6**, 041026 (2016).
  - [75] Y. Wang, L.-J. Lang, C. H. Lee, B. Zhang, and Y. D. Chong, Topologically enhanced harmonic generation in a nonlinear transmission line metamaterial, *Nat. Comm.* **10**, 1102 (2019).
  - [76] S. Krämer, D. Plankensteiner, L. Ostermann, and H. Ritsch, Quantumoptics.jl: A julia framework for simulating open quantum systems, *Computer Physics Communications* **227**, 109 (2018).



## Supplemental Materials

In these Supplemental Materials, we provide details of the analytic derivations based on the weak drive approximation, as well as details about the wave function Monte Carlo (WFMC) simulations.

### Weak drive approximation

The few-photon quantum states of a system of driven coupled nonlinear optical cavities can be calculated using the weak drive approximation, a method developed in earlier works [33, 35, 43]. The system's Hilbert space is divided into subspaces of different photon numbers, so that

$$|\psi\rangle = |\psi^{(0)}\rangle + |\psi^{(1)}\rangle + |\psi^{(2)}\rangle + \dots, \quad (\text{S1})$$

$$|\psi^{(k)}\rangle = \sum_{n_1 + \dots + n_N = k} c_{n_1 n_2 \dots n_N} |n_1, n_2, \dots, n_N\rangle, \quad (\text{S2})$$

where  $|n_1, n_2, \dots, n_N\rangle$  denotes the bosonic state with  $n_1$  photons on site 1,  $n_2$  photons on site 2, etc. The vacuum state is  $|\psi^{(0)}\rangle = |0, \dots, 0\rangle$ .

Amongst the various Hamiltonian terms discussed in the main text,  $\mathcal{H}_c$ ,  $\mathcal{H}'_p$ , and  $\mathcal{H}_{nl}$  all conserve photon number, but the driving Hamiltonian  $\mathcal{H}_d$  does not. Let us split  $\mathcal{H}_d$  as follows:

$$\mathcal{H}_d = \mathcal{H}_+ + \mathcal{H}_-, \quad (\text{S3})$$

$$\mathcal{H}_+ = \sum_{j=1}^N F_j a_j^\dagger = \mathcal{H}_-^\dagger. \quad (\text{S4})$$

In the weak drive limit, the amplitudes for higher photon number states are of sub-leading order, so

$$\langle \psi^{(k)} | \mathcal{H}_- | \psi^{(k+1)} \rangle \ll \langle \psi^{(k)} | \mathcal{H}_+ | \psi^{(k-1)} \rangle. \quad (\text{S5})$$

By matching particle number subspaces in the Schrödinger equation, we obtain

$$i\hbar \frac{d}{dt} |\psi^{(k)}\rangle = \mathcal{H} |\psi^{(k)}\rangle + \mathcal{H}_+ |\psi^{(k-1)}\rangle + \mathcal{H}_- |\psi^{(k+1)}\rangle \quad (\text{S6})$$

$$\approx \mathcal{H} |\psi^{(k)}\rangle + \mathcal{H}_+ |\psi^{(k-1)}\rangle. \quad (\text{S7})$$

Truncating at  $k = 2$  (i.e., neglecting states with three or more photons) gives

$$\begin{cases} i\hbar \frac{d}{dt} |\psi^{(1)}\rangle = \mathcal{H} |\psi^{(1)}\rangle + \mathcal{H}_+ |\psi^{(0)}\rangle, \\ i\hbar \frac{d}{dt} |\psi^{(2)}\rangle = \mathcal{H} |\psi^{(2)}\rangle + \mathcal{H}_+ |\psi^{(1)}\rangle. \end{cases} \quad (\text{S8})$$

We look for steady state solutions, for which the time derivatives are zero. Hence,

$$\begin{cases} |\psi^{(1)}\rangle = -\mathcal{H}^{-1} \mathcal{H}_+ |\psi^{(0)}\rangle \\ |\psi^{(2)}\rangle = -\mathcal{H}^{-1} \mathcal{H}_+ |\psi^{(1)}\rangle. \end{cases} \quad (\text{S10})$$

$$\begin{cases} |\psi^{(1)}\rangle = -\mathcal{H}^{-1} \mathcal{H}_+ |\psi^{(0)}\rangle \\ |\psi^{(2)}\rangle = -\mathcal{H}^{-1} \mathcal{H}_+ |\psi^{(1)}\rangle. \end{cases} \quad (\text{S11})$$

### Single-photon states

We can solve Eq. (S10) by using the lattice's eigenmode basis. Let  $|j\rangle \equiv a_j^\dagger |\psi^{(0)}\rangle$  be the state in which only site  $j$  is occupied, with a single photon. Projecting into the single-photon subspace and using these states as the basis, the Hamiltonian is

$$\mathcal{H}^{(1)} = z\mathcal{I} + \mathcal{H}_c^{(1)}, \quad \text{where} \quad (\text{S12})$$

$$z = E - i\frac{\gamma}{2}, \quad \mathcal{H}_c^{(1)} = \left( \sum_{j=1}^{N/2} |2j-1\rangle \langle 2j| + t \sum_{j=1}^{N/2-1} |2j\rangle \langle 2j+1| \right) + \text{h.c.}, \quad (\text{S13})$$



with  $\mathcal{I}$  denoting the identity operator. Note that  $\mathcal{H}_{nl}$  does not contribute at the single-photon level.

Denote the eigenstates of the single particle Hamiltonian  $\mathcal{H}_c^{(1)}$  by  $\{|\varphi_n\rangle\}$ , with the corresponding energy eigenvalues  $\{\epsilon_n\}$ . Using these eigenstates as an orthogonal basis for the single-particle Hilbert space, we obtain

$$\mathcal{H}^{(1)} |\varphi_n\rangle = (z + \epsilon_n) |\varphi_n\rangle. \quad (\text{S14})$$

Hence, the resolvent operator (or Green's function) can be written as

$$\mathcal{G}^{(1)} \equiv \left( z\mathcal{I} + \mathcal{H}_c^{(1)} \right)^{-1} = \sum_n \frac{|\varphi_n\rangle \langle \varphi_n|}{z + \epsilon_n}. \quad (\text{S15})$$

Plugging this into Eq. (S10) yields

$$|\psi^{(1)}\rangle = - \sum_{j=1}^N F_j \mathcal{G}^{(1)} |j\rangle \quad (\text{S16})$$

$$= - \sum_n \frac{f_n |\varphi_n\rangle}{z + \epsilon_n}, \quad \text{where } f_n = \sum_{j=1}^N F_j \langle \varphi_n | j \rangle. \quad (\text{S17})$$

### Two-photon states: linear limit

Next, we deal with the two-photon part of the weak drive solution, which is given by Eq. (S11). The two-particle subspace can be spanned using tensor product states such as  $|i, j\rangle = |i\rangle \otimes |j\rangle$  (site basis) or  $|\varphi_{kl}\rangle = |\varphi_k\rangle \otimes |\varphi_l\rangle$  (single-particle eigenbasis). Note that the basis vectors are not symmetrized, but the two-photon states themselves should be symmetrized, e.g.  $\langle i, j | \psi^{(2)} \rangle = \langle j, i | \psi^{(2)} \rangle$ .

Using Eq. (S16),

$$\mathcal{H}_+ |\psi^{(1)}\rangle = -\mathcal{H}_+ \sum_{j,j'} F_j |j'\rangle \langle j' | \mathcal{G}^{(1)} | j \rangle \quad (\text{S18})$$

$$= - \sum_{i,j,j'} \left( F_i a_i^\dagger \right) \left( F_j a_{j'}^\dagger |\psi^{(0)}\rangle \langle j' | \mathcal{G}^{(1)} | j \rangle \right) \quad (\text{S19})$$

$$= - \frac{1}{\sqrt{2}} \sum_{i,j} F_i F_j \left( |i\rangle \otimes \mathcal{G}^{(1)} |j\rangle + \mathcal{G}^{(1)} |j\rangle \otimes |i\rangle \right). \quad (\text{S20})$$

In deriving Eq. (S20), we are careful to distinguish same-site and different-site excitations:  $a_i^\dagger a_i^\dagger |\psi^{(0)}\rangle = \sqrt{2} |i, i\rangle$ , whereas  $a_i^\dagger a_j^\dagger |\psi^{(0)}\rangle = \frac{1}{\sqrt{2}} (|i, j\rangle + |j, i\rangle)$  for  $i \neq j$ . Hence, in the eigenstate basis,

$$\mathcal{H}_+ |\psi^{(1)}\rangle = - \frac{1}{\sqrt{2}} \sum_{mn} f_m f_n \frac{2z + \epsilon_m + \epsilon_n}{(z + \epsilon_m)(z + \epsilon_n)} |\varphi_{mn}\rangle. \quad (\text{S21})$$

Next, let us take the linear limit for the moment (i.e., neglecting  $\mathcal{H}_{nl}$ ). The projection of the Hamiltonian into the two-particle subspace is

$$\mathcal{H}_0^{(2)} = \mathcal{H}^{(1)} \otimes \mathcal{I} + \mathcal{I} \otimes \mathcal{H}^{(1)}, \quad (\text{S22})$$

and so, in the basis formed by the eigenstates,

$$\begin{aligned} \mathcal{H}_0^{(2)} |\varphi_{mn}\rangle &= \left( \mathcal{H}^{(1)} \otimes \mathcal{I} + \mathcal{I} \otimes \mathcal{H}^{(1)} \right) |\varphi_m\rangle \otimes |\varphi_n\rangle \\ &= (2z + \epsilon_m + \epsilon_n) |\varphi_{mn}\rangle. \end{aligned} \quad (\text{S23})$$

Hence, the two-photon Green's function, in the linear limit, is

$$\mathcal{G}_0^{(2)} \equiv \left( \mathcal{H}_0^{(2)} \right)^{-1} = \sum_{mn} \frac{|\varphi_{mn}\rangle \langle \varphi_{mn}|}{2z + \epsilon_m + \epsilon_n}. \quad (\text{S24})$$

Plugging Eqs. (S24) and (S21) into Eq. (S11), we obtain the two-photon state in the linear limit:

$$|\psi_0^{(2)}\rangle = \frac{1}{\sqrt{2}} \sum_{mn} \frac{f_m f_n}{(z + \epsilon_m)(z + \epsilon_n)} |\varphi_{mn}\rangle \quad (\text{S25})$$

$$= \frac{1}{\sqrt{2}} \left( \sum_m \frac{f_m}{z + \epsilon_m} |\varphi_m\rangle \right) \otimes \left( \sum_n \frac{f_n}{z + \epsilon_n} |\varphi_n\rangle \right) \quad (\text{S26})$$

$$= \frac{1}{\sqrt{2}} |\psi^{(1)}\rangle \otimes |\psi^{(1)}\rangle. \quad (\text{S27})$$

Hence, in the linear limit, the the zero delay time second order correlation functions are unity, as expected:

$$g_{ij}^{(2)}(0) \Big|_{\alpha=0} = 2 \left| \frac{\langle i, j | \psi_0^{(2)} \rangle}{\langle i | \psi^{(1)} \rangle \langle j | \psi^{(1)} \rangle} \right|^2 = 1. \quad (\text{S28})$$

### Two-photon states: perturbative correction

We now have to deal with the nonlinear term

$$\mathcal{H}_{nl}^{(2)} = 2\alpha \sum_i |i, i\rangle \langle i, i| \equiv \alpha \mathcal{V}. \quad (\text{S29})$$

For small  $\alpha$ , this can be treated perturbatively using the Dyson series:

$$\mathcal{G}^{(2)} \equiv \left( \mathcal{H}^{(2)} \right)^{-1} = \left( \mathcal{H}_0^{(2)} + \alpha \mathcal{V} \right)^{-1} = \mathcal{G}_0^{(2)} - \alpha \mathcal{G}_0^{(2)} \mathcal{V} \mathcal{G}_0^{(2)} + \dots \quad (\text{S30})$$

Truncating away the terms denoted by ellipses, and plugging back into Eq. (S11), gives the result

$$|\psi^{(2)}\rangle \approx |\psi_0^{(2)}\rangle + \alpha |\psi_1^{(2)}\rangle, \quad (\text{S31})$$

$$|\psi_0^{(2)}\rangle = \frac{1}{\sqrt{2}} |\psi^{(1)}\rangle \otimes |\psi^{(1)}\rangle \quad (\text{S32})$$

$$|\psi_1^{(2)}\rangle = \sum_{imnpq} \frac{-\sqrt{2} f_p f_q \langle \varphi_{mn} | i, i \rangle \langle i, i | \varphi_{pq} \rangle}{(z + \epsilon_p)(z + \epsilon_q)(2z + \epsilon_m + \epsilon_n)} |\varphi_{mn}\rangle. \quad (\text{S33})$$

$$= -\sqrt{2} \sum_{ijj'} F_j F_{j'} \mathcal{G}_0^{(2)} |i, i\rangle \langle i | \mathcal{G}^{(1)} |j\rangle \langle i | \mathcal{G}^{(1)} |j'\rangle. \quad (\text{S34})$$

In deriving Eq. (S33), we have combined Eqs. (S24), (S21), and (S29).

### Matrix elements of the single-photon Green's function

In Eq. (S15), we expressed the single-photon resolvent (S15) using the eigenbasis of the single-particle SSH Hamiltonian  $\mathcal{H}_c^{(1)}$ , defined in Eq. (S13). Within the disk  $|z| < 1$ , it can be further expanded as a Laurent series, as follows:

$$\mathcal{G}^{(1)} = \sum_n \frac{|\varphi_n\rangle \langle \varphi_n|}{z + \epsilon_n} = \sum_n \epsilon_n^{-1} \left( 1 + \frac{z}{\epsilon_n} \right)^{-1} |\varphi_n\rangle \langle \varphi_n| \quad (\text{S35})$$

$$= \sum_n \left( \epsilon_n^{-1} - \epsilon_n^{-2} z + \epsilon_n^{-3} z^2 - \dots \right) |\varphi_n\rangle \langle \varphi_n| \quad (\text{S36})$$

$$= g_c - z g_c^2 + z^2 g_c^3 - \dots, \quad (\text{S37})$$

where

$$g_c \equiv \left( \mathcal{H}_c^{(1)} \right)^{-1}. \quad (\text{S38})$$

We will need the matrix elements of  $g_c$ . For this, it is useful to write the SSH Hamiltonian in matrix form as

$$\mathcal{H}_c^{(1)} = \begin{bmatrix} 0 & 1 & & \\ 1 & 0 & t & \\ & t & 0 & 1 \\ & & 1 & 0 & \ddots \\ & & & \ddots & \ddots \end{bmatrix}_{N \times N} = H_0 + tH_1, \quad (\text{S39})$$

where

$$H_0 = \begin{bmatrix} A & & \\ & A & \\ & & A \\ & & & \ddots \end{bmatrix}, \quad H_1 = \begin{bmatrix} 0 & B & & \\ B^T & 0 & B & \\ & B^T & 0 & \ddots \\ & & \ddots & \ddots \end{bmatrix}, \quad A = \begin{bmatrix} 0 & 1 \\ 1 & 0 \end{bmatrix}, \quad B = \begin{bmatrix} 0 & 0 \\ 1 & 0 \end{bmatrix}. \quad (\text{S40})$$

For brevity, we denote

$$U = AB = \begin{bmatrix} 1 & 0 \\ 0 & 0 \end{bmatrix}, \quad D = AB^T = \begin{bmatrix} 0 & 0 \\ 0 & 1 \end{bmatrix}. \quad (\text{S41})$$

These matrices have the following easily-verified properties:

$$H_0 = H_0^{-1} \quad (\text{S42})$$

$$D^2 = D \quad (\text{S43})$$

$$U^2 = U \quad (\text{S44})$$

$$UD = DU = 0. \quad (\text{S45})$$

Moreover,

$$H_0 H_1 = \begin{bmatrix} 0 & U & & \\ D & 0 & U & \\ & D & 0 & U \\ & & D & 0 & \ddots \\ & & & \ddots & \ddots \end{bmatrix}, \quad (H_0 H_1)^2 = \begin{bmatrix} 0 & 0 & U & & \\ 0 & 0 & 0 & U & \\ D & 0 & 0 & 0 & \ddots \\ & D & 0 & 0 & \ddots \\ & & \ddots & \ddots & \ddots \end{bmatrix} \quad \dots \quad (H_0 H_1)^{N/2-1} = \begin{bmatrix} 0 & 0 & \dots & 0 & U \\ 0 & 0 & & 0 & \\ \vdots & & \ddots & & \vdots \\ 0 & & & 0 & 0 \\ D & 0 & \dots & 0 & 0 \end{bmatrix}. \quad (\text{S46})$$

For any  $n > N/2 - 1$ ,  $(H_0 H_1)^n = 0$ .

We now seek the following matrix element for each of the terms in the Laurent series (S37):

$$\langle N-1 | g_c^{m+1} | 1 \rangle, \quad m = 0, 1, 2, \dots,$$

with  $g_c$  defined in Eq. (S38). These are the matrix elements connecting the driven site,  $j = 1$ , and the signal site,  $j = N - 1$ . We will work in the small  $t$  regime, and look for solutions to lowest non-vanishing order in  $t$ . Using Eqs. (S39) and (S42),  $g_c$  can be expressed as a series in  $t$ :

$$g_c = (H_0 + tH_1)^{-1} = H_0 \sum_{n=0}^{\infty} (-tH_0 H_1)^n. \quad (\text{S47})$$

Now, for the zeroth-order term in the Laurent series,

$$\langle N-1 | g_c | 1 \rangle = \sum_{n=0}^{\infty} (-t)^n \langle N-1 | H_0 (H_0 H_1)^n | 1 \rangle. \quad (\text{S48})$$

Referring to Eq. (S46), all terms with  $n < N/2 - 1$  have vanishing matrix element (roughly speaking, there are not enough “powers of  $t$ ” to propagate from the first unit cell to the last unit cell). As for the next term, which is of order

$$n = N/2 - 1,$$

$$\langle N-1 | H_0 (H_0 H_1)^{N/2-1} | 1 \rangle = [0 \ \cdots \ 0 \ \langle +z |] \begin{bmatrix} A & & \\ & A & \\ & & \ddots \\ & & & A \end{bmatrix} \begin{bmatrix} 0 & \cdots & 0 & U \\ 0 & & & 0 \\ \vdots & \ddots & & \vdots \\ D & \cdots & 0 & 0 \end{bmatrix} \begin{bmatrix} | +z \rangle \\ 0 \\ \vdots \\ 0 \end{bmatrix} \quad \text{where } | +z \rangle \equiv \begin{bmatrix} 1 \\ 0 \end{bmatrix} \quad (\text{S49})$$

$$= [0 \ \cdots \ 0 \ \langle +z |] \begin{bmatrix} 0 \\ \vdots \\ 0 \\ AD | +z \rangle \end{bmatrix} \quad (\text{S50})$$

$$= \begin{bmatrix} 1 & 0 \end{bmatrix} \begin{bmatrix} 0 & 1 \\ 0 & 0 \end{bmatrix} \begin{bmatrix} 1 \\ 0 \end{bmatrix} = 0. \quad (\text{S51})$$

Hence,

$$\langle N-1 | g_c | 1 \rangle \sim O\left(t^{\frac{N}{2}}\right). \quad (\text{S52})$$

We now proceed to the  $O(z^1)$  term in the Laurent series. For this, we need to consider the double series

$$g_c^2 = \left( H_0 \sum_{n=0}^{\infty} (-t H_0 H_1)^n \right)^2 = \sum_{n=0}^{\infty} (-t)^n \sum_{p=0}^n H_0 (H_0 H_1)^p H_0 (H_0 H_1)^{n-p}. \quad (\text{S53})$$

Referring again to Eq. (S46), the terms with  $n < N/2 - 1$  have vanishing  $(N-1, 1)$  matrix element. The matrix element for the next order term is

$$(-t)^{\frac{N}{2}-1} \sum_{p=0}^{N/2-1} \langle N-1 | H_0 (H_0 H_1)^p H_0 (H_0 H_1)^{\frac{N}{2}-1-p} | 1 \rangle.$$

For each  $p$ , we can evaluate the matrix expressions similarly to Eqs (S49)–(S51). Because  $ADAD = 0$ , it turns out that the only non-vanishing term is  $p = N/2 - 1$ :

$$\langle N-1 | H_0 (H_0 H_1)^{\frac{N}{2}-1} H_0 | 1 \rangle = \langle +z | ADA | +z \rangle = 1 \quad (\text{S54})$$

$$\Rightarrow \langle N-1 | g_c^2 | 1 \rangle = (-t)^{\frac{N}{2}-1} + O\left(t^{\frac{N}{2}}\right). \quad (\text{S55})$$

Notably, the leading term is lower order in  $t$  than the contribution from the zeroth-order Laurent series term, Eq. (S52).

It can similarly be seen that the higher order terms in the Laurent series, involving  $g_c^3$ ,  $g_c^4$ , and so forth, all have vanishing contributions to order  $t^{N/2-1}$  or below. Thus,

$$\langle N-1 | \mathcal{G}^{(1)} | 1 \rangle = -z(-t)^{\frac{N}{2}-1} + O\left(t^{\frac{N}{2}}\right). \quad (\text{S56})$$

This expression is valid to lowest order in  $t$ , but to *all* orders in  $z$  within the circle of convergence  $|z| < 1$ .

### Photon blockade condition

We now return to the two-photon wavefunctions, whose two leading terms are given by Eqs. (S31)–(S33).

First, consider the zeroth-order term (S32), and consider the two-photon amplitude in the signal resonator, under the driving condition  $f_n = F_1 \langle \varphi_n | 1 \rangle$ . From Eqs. (S16) and (S27),

$$\langle N-1, N-1 | \psi_0^{(2)} \rangle = \frac{1}{\sqrt{2}} \langle N-1, N-1 | \left( |\psi^{(1)}\rangle \otimes |\psi^{(1)}\rangle \right) \rangle \quad (\text{S57})$$

$$= \frac{F_1^2}{\sqrt{2}} \left( \langle N-1 | \mathcal{G}^{(1)} | 1 \rangle \right)^2 \quad (\text{S58})$$

Hence, using Eq. (S56),

$$\langle N-1, N-1 | \psi_0^{(2)} \rangle \approx \frac{F_1^2}{\sqrt{2}} z^2 t^{N-2}. \quad (\text{S59})$$

Next, we turn to the first-order term (S33). Before taking the matrix elements, let us perform a few simplifications:

$$|\psi_1^{(2)}\rangle = \sum_{imnpq} |\varphi_{mn}\rangle \frac{-\sqrt{2}f_p f_q \langle \varphi_{mn} | i, i \rangle \langle i, i | \varphi_{pq} \rangle}{(z + \epsilon_p)(z + \epsilon_q)(2z + \epsilon_m + \epsilon_n)} \quad (\text{S60})$$

$$= -\sqrt{2}F_1^2 \sum_{imn} \langle i, i | \sum_{pq} \frac{|\varphi_{pq}\rangle \langle \varphi_{pq}|}{(z + \epsilon_p)(z + \epsilon_q)} | 1, 1 \rangle \frac{\langle \varphi_{mn} | i, i \rangle}{2z + \epsilon_m + \epsilon_n} |\varphi_{mn}\rangle \quad (\text{S61})$$

$$= -\sqrt{2}F_1^2 \sum_{imn} \frac{[\langle i | \mathcal{G}^{(1)} | 1 \rangle]^2 \langle \varphi_{mn} | i, i \rangle}{2z + \epsilon_m + \epsilon_n} |\varphi_{mn}\rangle \quad (\text{S62})$$

The  $\langle i | \mathcal{G}^{(1)} | 1 \rangle$  in the numerator can be evaluated to lowest order in  $t$ . Referring back to Eqs. (S37) and (S47), only the  $i = 2$  case yields a zeroth order contribution:

$$\langle i | \mathcal{G}^{(1)} | 1 \rangle = \langle i | (g_c + \dots) | 1 \rangle = \langle i | H_0 | 1 \rangle + \dots = \delta_{i2} + \dots, \quad (\text{S63})$$

where ellipses denote terms of  $O(t)$  and higher. Hence,

$$|\psi_1^{(2)}\rangle \approx -\sqrt{2}F_1^2 \sum_{mn} \frac{|\varphi_{mn}\rangle \langle \varphi_{mn} | 2, 2 \rangle}{2z + \epsilon_m + \epsilon_n} \quad (\text{S64})$$

$$= -\sqrt{2}F_1^2 \left( \sum_{\epsilon_m \epsilon_n > 0} + \sum_{\epsilon_m \epsilon_n < 0} \right) \frac{|\varphi_{mn}\rangle \langle \varphi_{mn} | 2, 2 \rangle}{2z + \epsilon_m + \epsilon_n} \quad (\text{S65})$$

In the last line, we have split the sums over eigenstates to account for the fact that the single-particle SSH model has both positive- and negative-energy states. The model's chiral symmetry ensures that the eigenstates occur in pairs with energies of opposite signs. Evidently, the largest contributions in the above sums come from the terms with  $\epsilon_m$  and  $\epsilon_n$  of opposite signs, so that they can (partially or fully) cancel each other in the denominator:

$$|\psi_1^{(2)}\rangle \approx -\sqrt{2}F_1^2 \sum_{\epsilon_m \epsilon_n < 0} \frac{|\varphi_{mn}\rangle \langle \varphi_{mn} | 2, 2 \rangle}{2z + \epsilon_m + \epsilon_n}. \quad (\text{S66})$$

Referring to Eqs. (S39)–(S40), we can write

$$\langle \varphi_n | 2 \rangle = \langle \varphi_n | H_0 | 1 \rangle = \langle \varphi_n | (\mathcal{H}_c^{(1)} - tH_1) | 1 \rangle = \epsilon_n \langle \varphi_n | 1 \rangle. \quad (\text{S67})$$

Plugging this into Eq. (S66) gives

$$|\psi_1^{(2)}\rangle \approx -\sqrt{2}F_1^2 \sum_{\epsilon_m \epsilon_n < 0} \frac{\epsilon_m \epsilon_n |\varphi_{mn}\rangle \langle \varphi_{mn} | 1, 1 \rangle}{2z + \epsilon_m + \epsilon_n}. \quad (\text{S68})$$

Hence,

$$\langle N-1, N-1 | \psi_1^{(2)} \rangle = -\sqrt{2}F_1^2 \left[ \sum_{\epsilon_m < 0} \sum_{\epsilon_n > 0} \frac{A_{mn}}{2z + \epsilon_m + \epsilon_n} + \sum_{\epsilon_m > 0} \sum_{\epsilon_n < 0} \frac{A_{mn}}{2z + \epsilon_m + \epsilon_n} \right], \quad (\text{S69})$$

$$A_{mn} = \epsilon_m \epsilon_n \langle N-1 | \varphi_m \rangle \langle \varphi_m | 1 \rangle \langle N-1 | \varphi_n \rangle \langle \varphi_n | 1 \rangle. \quad (\text{S70})$$

The chiral symmetry operator

$$\Gamma = \begin{bmatrix} 1 & & & \\ & -1 & & \\ & & 1 & \\ & & & -1 \\ & & & & \ddots \\ & & & & & \ddots \end{bmatrix}_{N \times N} \quad (\text{S71})$$

anticommutes with  $\mathcal{H}_c^{(1)}$  and maps each eigenstate to one with an eigenvalue of the opposite sign:

$$\mathcal{H}_c^{(1)} \Gamma |\varphi_n\rangle = -\epsilon_n \Gamma |\varphi_n\rangle. \quad (\text{S72})$$

Using this, we can replace the sum over the negative-energy states in Eq. (S69) (say index  $n$ ) with a sum over positive energy states, with the terms in the sum modified by replacing  $|n\rangle$  with  $\Gamma|n\rangle$  and  $\epsilon_n$  with  $-\epsilon_n$ . It is easily shown that the  $A_{mn}$  factor switches sign in the process, so that

$$\langle N-1, N-1 | \psi_1^{(2)} \rangle = \sqrt{2} F_1^2 \sum_{\epsilon_m, \epsilon_n > 0} A_{mn} \left[ \frac{1}{2z + (\epsilon_m - \epsilon_n)} + \frac{1}{2z - (\epsilon_m - \epsilon_n)} \right] \quad (\text{S73})$$

For an infinite dimer chain, the width of the upper band is  $2t$ . For a finite chain, we have  $|\epsilon_m - \epsilon_n| \lesssim 2t$  for  $\epsilon_m, \epsilon_n > 0$ . For  $|z| > t$ , we can take the Laurent expansion

$$\langle N-1, N-1 | \psi_1^{(2)} \rangle = 2\sqrt{2} F_1^2 \sum_{\epsilon_m, \epsilon_n > 0} \frac{A_{mn}}{2z} \sum_{p=0}^{\infty} \left( \frac{\epsilon_m - \epsilon_n}{2z} \right)^{2p} \quad (\text{S74})$$

$$= 2\sqrt{2} F_1^2 \sum_{p=0}^{\infty} (2z)^{-(2p+1)} \sum_{\epsilon_m, \epsilon_n > 0} A_{mn} (\epsilon_m - \epsilon_n)^{2p}. \quad (\text{S75})$$

The inner sum in Eq. (S75) can be evaluated with the help of Eq. (S70):

$$\sum_{\epsilon_m, \epsilon_n > 0} A_{mn} (\epsilon_m - \epsilon_n)^{2p} = \sum_{\epsilon_m, \epsilon_n > 0} A_{mn} \sum_{h=0}^{2p} (-1)^h \binom{2p}{h} \epsilon_m^{2p-h} \epsilon_n^h \quad (\text{S76})$$

$$= \sum_{\epsilon_m, \epsilon_n > 0} \langle N-1 | \varphi_m \rangle \langle \varphi_m | 1 \rangle \langle N-1 | \varphi_n \rangle \langle \varphi_n | 1 \rangle \sum_{h=0}^{2p} (-1)^h \binom{2p}{h} \epsilon_m^{2p-h+1} \epsilon_n^{h+1} \quad (\text{S77})$$

$$= \sum_{h=0}^{2p} (-1)^h \binom{2p}{h} \langle N-1 | (\mathcal{H}_c^+)^{2p-h+1} | 1 \rangle \langle N-1 | (\mathcal{H}_c^+)^{h+1} | 1 \rangle, \quad (\text{S78})$$

where

$$\mathcal{H}_c^+ = \sum_{\epsilon_n > 0} \epsilon_n |\varphi_n\rangle \langle \varphi_n|. \quad (\text{S79})$$

Similar to our earlier treatment of  $\mathcal{H}_c^{(1)}$ , we can show that

$$\langle N-1 | (\mathcal{H}_c^+)^{\nu} | 1 \rangle = \frac{1}{2} G(N-2, \nu) t^{\frac{N}{2}-1} + O(t^{\frac{N}{2}}), \quad (\text{S80})$$

where

$$G(a, b) \equiv \frac{b!!}{a!!(b-a)!!}. \quad (\text{S81})$$

Applying this to Eq. (S78) yields

$$\sum_{\epsilon_m, \epsilon_n > 0} A_{mn} (\epsilon_m - \epsilon_n)^{2p} = \frac{t^{N-2}}{4} \sum_{h=0}^{2p} (-1)^h \binom{2p}{h} G(N-2, 2p-h+1) G(N-2, h+1) + O(t^{N-1}). \quad (\text{S82})$$

It can be proven that the sum is zero for  $2p \geq N$ , whereas for  $2p = N-2$ ,

$$\sum_{h=0}^{N-2} (-1)^h \binom{N-2}{h} G(N-2, N-h-1) G(N-2, h+1) = (-1)^{\frac{N}{2}+1} \frac{(N-3)!!}{(N-2)!!}. \quad (\text{S83})$$

Plugging this back into Eqs. (S75) and (S78) yields, to lowest order in  $z$  and  $t$ ,

$$\langle N-1, N-1 | \psi_1^{(2)} \rangle \approx \frac{(-1)^{\frac{N}{2}+1} F_1^2 (N-3)!!}{\sqrt{2}} \frac{t^{N-2}}{(N-2)!! (2z)^{N-1}}. \quad (\text{S84})$$

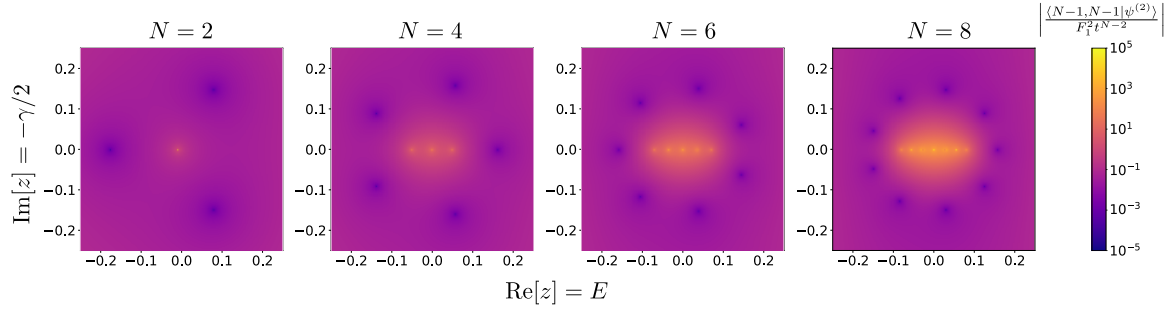


FIG. S1. Normalized two-photon signal  $|\langle N-1, N-1 | \psi^{(2)} \rangle / (F_1^2 t^{N-2})|$  for  $N = 2, 4, 6$ , and  $8$ , calculated using the weak drive equations. Parameters used here are the same as in Fig. 2 for each  $N$ . Compared to  $g_s^{(2)}(0)$ , which is featured in the other plots, this quantity omits the effects of variations in the single-photon amplitudes.

Hence, by combining Eqs. (S31), (S59), and (S84), we obtain an expression for the two-photon state  $|\psi^{(2)}\rangle$ . The amplitude on the signal site  $N-1$  is plotted in Fig. S1 for different choices of  $N$ .

Finally, we see that  $|\psi^{(2)}\rangle = 0$  when

$$\alpha \approx \frac{(-1)^{\frac{N}{2}} (N-2)!!}{4 (N-3)!!} (2z)^{N+1}, \quad (\text{S85})$$

which is the UPB condition given in the main text.

The photon occupation number on the signal site  $N-1$  is

$$n_{N-1} = \left| \langle N-1 | \psi^{(1)} \rangle \right|^2 \quad (\text{S86})$$

$$= \left| \langle N-1 | \psi^{(1)} \rangle \langle N-1 | \psi^{(1)} \rangle \right| \quad (\text{S87})$$

$$= \left| \sqrt{2} \langle N-1, N-1 | \psi_0^{(2)} \rangle \right| \quad (\text{S88})$$

$$= F_1^2 t^{N-2} |z|^2. \quad (\text{S89})$$

### WFMC Simulations

The Wave function Monte Carlo (WFMC) or “quantum trajectory” calculations [66] reported in this work were performed using the `QuantumOptics.jl` toolbox [76]. The WFMC calculations take place in a tensor product space of the truncated Fock spaces for the different lattice sites. Due to the combination of weak driving and uneven photon occupations, we found it necessary to take the following steps to ensure that the results are accurate:

- Direct inclusion of the recycling terms in terms of jumps would make their rate very small, due to the low photon occupations, yet their effect may not necessarily be negligible. Given the finite statistics generated by the Monte Carlo simulations, this would likely result in a bad sampling of rare events. To overcome this, we note that a master equation described by a Hamiltonian  $\mathcal{H}$  and jump operators  $= \{L_j^1, L_j^2\} = \{\sqrt{\gamma}a_j, \sqrt{\kappa}a_j^\dagger a_j\}$  can be rewritten with a simultaneous transformation

$$\mathcal{H} \rightarrow \mathcal{H}' = \mathcal{H} + \frac{\beta}{2i} \sum_j \left( \sqrt{\gamma}a_j + \sqrt{\kappa}a_j^\dagger a_j - \text{h.c.} \right) \quad (\text{S90})$$

$$L_j^1 \rightarrow L_j^{1'} = \sqrt{\gamma}a_j + \beta \mathbf{1} \quad (\text{S91})$$

$$L_j^2 \rightarrow L_j^{2'} = \sqrt{\kappa}a_j^\dagger a_j + \beta \mathbf{1}, \quad (\text{S92})$$

where  $\beta$  is an arbitrary constant. Even though this master equation generates the same evolution, the behaviour of individual trajectories can be very different as the jump rates increase from  $\langle L^\dagger L \rangle$  to  $\langle L'^\dagger L' \rangle$ . This procedure is known as “choosing a different unraveling” [66]. The limit  $\beta \rightarrow \infty$  leads to a diffusion process corresponding to homodyne detection. In our WFMC simulations, we take  $\beta = 0.1$ .



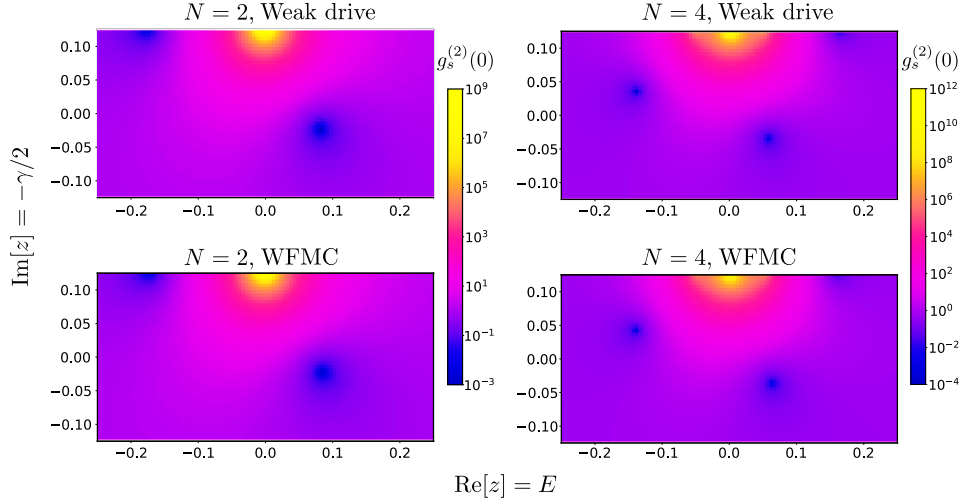


FIG. S2. WPMC verification of weak drive limit result for lattice sizes  $N = 2$  and  $N = 4$ . The color of the heat map corresponds to  $g_s^{(2)}(0)$ . The Kerr coefficients are  $\alpha = 10^{-2}$  for  $N = 2$  and  $2 \times 10^{-3}$  for  $N = 4$ ; all other parameters are the same as in Fig. 3(a) of the main text.

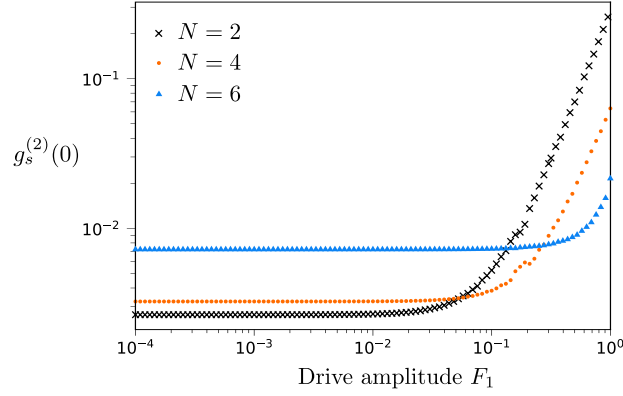


FIG. S3. WPMC calculations of  $g_s^{(2)}$  for different values of the drive amplitude  $F_1$ , with lattice sizes  $N = 2, 4$ , and  $6$ . The other parameters are the same as in previous simulations:  $t = 0.1$  and  $\alpha = 10^{-2}, 2 \times 10^{-3}, 2 \times 10^{-4}$  for  $N = 2, 4, 6$ . The values of  $z$  are chosen to be close to the optimal values for achieving UPB, as determined by searching for the minimum of  $g_s^{(2)}$  on a 2D grid (due to the discretization of the search grid, for each  $N$  the system is slightly detuned from the true optimum). Pure dephasing is not included.

- The numerical solver was run with strict tolerance settings. For the simulations with  $F = 10^{-4}$ , we used  $\text{RelTol} = \text{AbsTol} = 10^{-18}$ . For other values of  $F$ , we chose similar tolerances, based on what is required for convergence.
- To account for slow dynamics, the state was allowed to relax freely from the vacuum to the steady state during an initial time  $T_{\text{relax}}$ , and the results were recorded over a subsequent time  $T_{\text{record}}$ . The trajectory simulations were repeated  $N_{\text{traj}}$  times to allow for additional averaging and estimation of statistical error through jackknife resampling. In most of the simulations, we used  $T_{\text{relax}} = 10^3 \hbar$ ,  $T_{\text{record}} = 10^4 \hbar$  and  $N_{\text{traj}} = 10$ .
- We carefully chose the Fock cutoffs  $N_{\text{Fock}}^{(j)}$  (i.e., the maximal amount of photons allowed on each site  $j$ ). Appropriate choices for each  $j$  were needed to maintain accuracy while keeping the computational cost manageable. For the simulations at  $F = 10^{-4}$ , for example, we used  $N_{\text{Fock}}^{(j)} = 3$  for all  $j$ ; whereas to study the large- $F$  limit with  $N = 4$ , we took  $N_{\text{Fock}}^{(1)} = N_{\text{Fock}}^{(2)} = 32$  and  $N_{\text{Fock}}^{(3)} = N_{\text{Fock}}^{(4)} = 8$ .

In all cases, we verified that the values were sufficient for proper convergence.

In the main text, Fig. 3(a) plots the second-order correlation  $g_s^{(2)}$  shows for lattice size  $N = 6$ , comparing the results obtained from the weak drive equations and WPMC simulations (without pure dephasing). In Fig. S2, we show the

analogous plots for  $N = 2$  and  $N = 4$ . It can be seen that the weak drive equations and WFMC results are in good agreement for different values of  $N$ .

In all of the other WFMC results presented in this work, we chose a drive amplitude  $F_1 = 10^{-4}$  (in units of the lattice's intra-cell coupling). The weak drive equations rely on the assumption that the drive amplitude is small. In Fig. S3, we show the values of  $g_s^{(2)}$  produced by WFMC simulations with different values of  $F_1$ . It can be seen that for  $F_1 \lesssim 10^{-2}$ , the WFMC results become approximately independent of  $F$ , consistent with the existence of a well-defined weak drive limit.

### WFMC calculations of unequal-time correlation functions

Assuming that the system reaches a steady state with constant  $\langle n_j(t) \rangle$ , the time-dependent second-order correlation function at the  $j$ th lattice site can be defined as

$$g_j^{(2)}(\tau) = \frac{\langle a_j^\dagger(0) a_j^\dagger(\tau) a_j(\tau) a_j(0) \rangle}{\langle n_j(0) \rangle^2}. \quad (\text{S93})$$

To study this numerically, we again run the simulation over a time span  $T_{\text{relax}}$  to allow the state to relax to steady state. Subsequently, the expectation value for the denominator of Eq. (S93) is obtained over a span  $T_{\text{record}}^{\text{stat}}$ . After this, the state is  $|\psi_s(t_0)\rangle$ , where  $s = 1, \dots, N_{\text{traj}}$ . We then define

$$|\phi_s(t_0)\rangle = \frac{a_j |\psi_s(t_0)\rangle}{\|a_j |\psi_s(t_0)\rangle\|}, \quad (\text{S94})$$

and propagate the system for a time  $\tau$ . Then,

$$\begin{aligned} \left\langle a_j^\dagger(t_0) a_j^\dagger(t_0 + \tau) a_j(t_0 + \tau) a_j(t_0) \right\rangle_s &= \langle \phi_s(t_0 + \tau) | n_j | \phi_s(t_0 + \tau) \rangle \|a_j |\psi_s(t_0)\rangle\|^2 \\ &= \langle \phi_s(t_0 + \tau) | n_j | \phi_s(t_0 + \tau) \rangle \langle \psi_s(t_0) | n_j | \psi_s(t_0) \rangle. \end{aligned} \quad (\text{S95})$$

As we are interested in steady state properties (the time-offset  $t_0$  is unimportant), the numerator of Eq. (S93) is readily obtained by averaging Eq. (S95) over the different trajectories  $s$ .